

Systematic Studies of Early Actinide Complexes: Thorium(IV) Fluoroketimides

Eric J. Schelter, Ping Yang, Brian L. Scott, Ryan E. Da Re, Kimberly C. Jantunen, Richard L. Martin, P. Jeffrey Hay,* David E. Morris,* and Jaqueline L. Kiplinger*

Los Alamos National Laboratory, Los Alamos, New Mexico 87545

Received December 2, 2006; E-mail: kiplinger@lanl.gov

Abstract: Reaction of $(C_5Me_5)_2Th(CH_3)_2$ with 2 equiv of $N\equiv C-Ar_F$ gives the corresponding fluorinated thorium(IV) bis(ketimide) complexes $(C_5Me_5)_2Th[-N=C(CH_3)(Ar_F)]_2$ (where $Ar_F = 3-F-C_6H_4$ (**4**), $4-F-C_6H_4$ (**5**), $2-F-C_6H_4$ (**6**), $3,5-F_2-C_6H_3$ (**7**), $3,4,5-F_3-C_6H_2$ (**8**), $2,6-F_2-C_6H_3$ (**9**), $2,4,6-F_3-C_6H_2$ (**10**), and C_6F_5 (**11**)). The complexes have been characterized by a combination of single-crystal X-ray diffraction, cyclic voltammetry and NMR, and UV-visible absorption and low-temperature luminescence spectroscopies. Density functional theory (DFT) and time-dependent DFT (TD-DFT) results are reported for complexes **5**, **11**, and $(C_5Me_5)_2Th[-N=C(Ph)]_2$ (**1**) for comparison with experimental data and to guide in the interpretation of the spectroscopic results. The most significant structural perturbation imparted by the fluorine substitution in these complexes is a rotation of the fluorophenyl group (Ar_F) out of the plane defined by the $N=C(C_{Me})-(C_{ipso})$ fragment in complexes **9–11** when the Ar_F group possesses two ortho fluorine atoms. Excellent agreement is obtained between the optimized ground state DFT calculated structures and crystal structures for **11**, which displays the distortion, as well as **5**, which does not. In complexes **9–11**, the out-of-plane rotation results in large interplanar angles (ϕ) between the planes formed by ketimide atoms $N=C(C_{Me})-(C_{ipso})$ and the ketimide aryl groups in the range $\phi = 49.1\text{--}88.8^\circ$, while in complexes **5**, **7**, and **8**, $\phi = 5.7\text{--}34.9^\circ$. The large distortions in **9–11** are a consequence of an unfavorable steric interaction between one of the two ortho fluorine atoms and the methyl group $[-N=C(CH_3)]$ on the ketimide ligand. Excellent agreement is also observed between the experimental electronic spectroscopic data and the TD-DFT predictions that the two lowest lying singlet states are principally of nonbonding nitrogen p orbital to antibonding $C=N \pi^*$ orbital ($p_N \rightarrow \pi^*_{C=N}$ or $n\pi^*$) character, giving rise to moderately intense transitions in the mid-visible spectral region that are separated in energy by less than 0.1 eV. Low-temperature (77 K) luminescence from both singlet and triplet excited states are also observed for these complexes. Emission lifetime data at 77 K for the triplet states are in the range 50–400 μs . These emission spectral data also exhibit vibronic structure indicative of a small Franck-Condon distortion in the ketimide $M-N=C(R_1)(R_2)$ linkage. Consistent with this vibronic structure, resonance enhanced Raman vibrational scattering is also observed for $(C_5Me_5)_2Th[-N=C(Ph)(CH_2Ph)]_2$ (**2**) when exciting into the visible excited states. These systems represent rare examples of Th(IV) complexes that engender luminescence and resonance Raman spectral signatures.

Introduction

Organometallic actinide complexes containing metal–ligand multiple bonds continue to provide a useful platform for probing the involvement of 5f and 6d orbitals in bonding and the effects of such bonding on electronic structure. Bond orders greater than one engender tunable metal-based electronic properties due to strong interactions of ligand and 5f- and/or 6d-actinide valence orbitals.^{1–3} Recently, we reported that benzonitrile inserts into the actinide–carbon bonds in

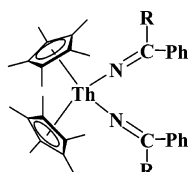
complexes of the type $(C_5Me_5)_2AnR_2$ to afford bis(ketimide) complexes $(C_5Me_5)_2An[-N=C(Ph)(R)]_2$ (where $An = Th, R = Ph, CH_2Ph, CH_3$; $An = U, R = CH_2Ph, CH_3$) and determined through structural, electrochemical, and spectroscopic studies that the $An-N$ interactions in these complexes possessed bond orders greater than one.^{3–5} As few systematic studies on the electronic structures across a homologous series of actinide complexes have been reported,^{6–9} we were interested in

- (1) Burns, C. J.; Eisen, M. S. In *The Chemistry of the Actinide and Transactinide Elements*, 3rd ed.; Morss, L. R., Edelstein, N. M., Fuger, J., Eds.; Springer: Dordrecht, 2006.
- (2) Ephritikhine, M. *Dalton Trans.* **2006**, 2501.
- (3) (a) Jantunen, K. C.; Burns, C. J.; Castro-Rodriguez, I.; Da Re, R. E.; Golden, J. T.; Morris, D. E.; Scott, B. L.; Taw, F. L.; Kiplinger, J. L. *Organometallics* **2004**, *23*, 4682. (b) Morris, D. E.; Da Re, R. E.; Jantunen, K. C.; Castro-Rodriguez, I.; Kiplinger, J. L. *Organometallics* **2004**, *23*, 5142. (c) Schelter, E. J.; Morris, D. E.; Scott, B. L.; Kiplinger, J. L. *Chem. Commun.* **2007**, 1029.

- (4) Kiplinger, J. L.; Morris, D. E.; Scott, B. L.; Burns, C. J. *Organometallics* **2002**, *21*, 3073.
- (5) Da Re, R. E.; Jantunen, K. C.; Golden, J. T.; Kiplinger, J. L.; Morris, D. E. *J. Am. Chem. Soc.* **2005**, *127*, 682.
- (6) Durakiewicz, T.; Joyce, J. J.; Lander, G. H.; Olson, C. G.; Butterfield, M. T.; Guziewicz, E.; Arko, A. J.; Morales, L.; Rebizant, J.; Mattenberger, K.; Vogt, O. *Phys. Rev. B: Condens. Matter* **2004**, *70*, 205103.
- (7) Cramer, R. E.; Roth, S.; Edelman, F.; Bruck, M. A.; Cohn, K. C.; Gilje, J. W. *Organometallics* **1989**, *8*, 1192.
- (8) Lukens, W. W.; Allen, P. G.; Bucher, J. J.; Edelstein, N. N.; Hudson, E. A.; Shuh, D. K.; Reich, T.; Andersen, R. A. *Organometallics* **1999**, *18*, 1253.

exploiting the $(C_5Me_5)_2An$ bis(ketimide) framework to prepare a series of complexes from fluorinated nitriles to tune electronic properties of the resulting complexes.

Our previous reports on the thorium bis(ketimide) complexes $(C_5Me_5)_2Th[-N=C(Ph)(R)]_2$ $R = Ph$ (**1**), CH_2Ph (**2**), or CH_3 (**3**) describe their intense yellow-to-orange colors.^{3a}



$R = Ph$ (**1**), CH_2Ph (**2**), CH_3 (**3**)

Toluene solutions of these complexes were found to have molar extinction coefficients in the visible region of $\sim 500 M^{-1} cm^{-1}$; such intensities in the visible region are quite unusual for complexes of the $6d^05f^0 Th(IV)$ ion.¹⁰ The electronic transitions responsible for the colors of the thorium bis(ketimide) species were subsequently assigned to ligand-centered non-bonding $p_N \rightarrow$ antibonding $\pi^*_{C=N}$ ($n\pi^*$) transitions, but the orbitals involved in these states were determined to contain contributions from metal-based valence orbitals.¹¹ Interestingly, this signature $n\pi^*$ electronic transition for **1** was found to be significantly red-shifted from that observed for **2** and **3**. This observation suggests that a strong substituent effect exists upon changing the R group of the ketimide ligand from the similar $-CH_3$ and $-CH_2Ph$ groups to $-Ph$, an effect that may be attributed to modulation of the thorium ketimide bonding interaction and/or the result of changes in the symmetry of the ketimide ligand itself.

Given these significant changes in the ligand-based electronic transitions for the thorium bis(ketimide) complexes **1–3** on changing from alkyl to phenyl substituents, we prepared a series of complexes designed to systematically perturb their electronic structure, perhaps even to the extent of inverting the ordering of energetically close d and f states of the $Th(IV)$ ion^{12,13} by virtue of the electron-withdrawing nature of the R substituent, thereby inducing new ground- and excited-electronic states derived from thorium f-orbital parentage. Herein we report a series of ketimide complexes possessing fluorinated aromatic groups with an eye toward establishing trends in their respective electronic structures based on electron-withdrawing ability. Detailed structural, electrochemical, and spectroscopic data have been obtained for this series to explore and quantify the manifestations of substituent-induced changes in electronic effects arising from the ketimide ligands. Results from density functional theory calculations are also reported for a subset of these complexes to guide the interpretation of the structural and spectroscopic data. Finally, we demonstrate that these thorium bis(ketimide) species are rare examples of tetravalent actinide-containing complexes that exhibit luminescence, with measured emission lifetimes at 77 K in the range of 50–400 μs , and also

engender resonance-enhanced Raman spectra when exciting into the visible electronic transitions.

Experimental Section

Instrumentation and Sample Protocols. Electronic absorption spectral data were obtained for toluene solutions of all complexes over the wavelength range 300–1600 nm on a Perkin-Elmer model Lambda 950 UV–visible–near-infrared spectrophotometer. All data were collected in 1-cm path length cuvettes loaded in a recirculating Vacuum Atmospheres model HE-553-2 inert atmosphere (N_2) drybox with a MO-40-2 Dri-Train and run versus a toluene reference. Spectral resolution was typically 2 nm.

Emission spectral data were collected on either a Spex Industries Fluorolog 2 system or a Photon Technology International (PTI) model QM-4 system. The former is comprised of a 450 W Xe arc lamp CW source, a 0.22-m single-stage excitation monochromator, a 0.22-m double emission monochromator, both with 1200 groove/mm gratings, and a thermoelectrically cooled Hamamatsu R928 photomultiplier detector. The PTI system comprises 0.2-m single-stage emission and excitation monochromators with 1200 groove/mm gratings. It can be implemented in either a continuous-wave excitation mode using a 75 W Xe arc lamp source, or a pulsed (time-resolved) excitation mode using a Xe flashlamp. Both CW and time-resolved detectors employ Hamamatsu R928 photomultiplier tubes. Spectral resolution in all emission scans was < 2 nm. Emission spectral samples were typically 1–10 mM in toluene or THF and were prepared in the Vacuum Atmospheres drybox system described above; data were collected on samples in flame-sealed medium-walled NMR tubes (Wilmad 504-PP) at 77 K as glasses or ices using a liquid-nitrogen-cooled optical dewar.

Resonance Raman spectra were obtained using excitation (λ_{ex}) from a Spectra Physics 2045 Ar-ion laser or an Ar-ion-pumped Coherent Radiation 599 dye laser charged with *trans*-stilbene. Scattered light was collected and directed into a Jobin Yvon HR640 spectrometer operated as a single-stage spectrograph equipped with an 1800 grooves/mm grating; the single-stage spectrograph requires that the scattered light be passed through a holographic notch filter (Kaiser) to reduce contributions from Rayleigh scattering. Typical resolution was $\sim 5 cm^{-1}$. For all excitation wavelengths, scattering intensities were recorded using a Princeton Instruments liquid-nitrogen-cooled CCD detector. A polarization scrambler was placed at the entrance slit of the spectrograph to minimize distortions in the observed scattering intensities due to wavelength-dependent instrument response to polarized light. Typical excitation powers and integration times were 20–50 mW and 15–120 min, respectively. Raman shifts were calibrated against an external reference of 4-acetamidophenol, and spectra were corrected by subtraction of a spectral baseline obtained with a spline-fitting procedure. The dispersion characteristics of our instrumentation typically require the acquisition and concatenation of several spectral windows to encompass the entire Raman shift range from ~ 150 to $1700 cm^{-1}$ (e.g., two windows are required for 457.9 nm excitation); windows were selected such that adjacent windows contained sufficient overlap of Raman bands to derive a continuous trace. Peak positions were determined by fitting band profiles. Samples for Raman studies were prepared using the same protocols described above for the emission spectral samples.

Cyclic voltammetric data were obtained in the Vacuum Atmospheres drybox system described above. All data were collected using a Perkin-Elmer Princeton Applied Research Corporation (PARC) model 263 potentiostat under computer control with PARC model 270 software. All sample solutions were ~ 5 mM in complex with 0.1 M $[Bu_4N][B(C_6F_5)_4]$ supporting electrolyte in THF solvent. All data were collected with the positive-feedback IR compensation feature of the software/potentiostat activated to minimize contribution to the voltammetric waves from uncompensated solution resistance (typically $\sim 1 k\Omega$ under the conditions employed). Solutions were contained in PARC model K0264 microcells consisting of a ~ 3 -mm diameter Pt disk working electrode, a Pt wire counter electrode, and a silver wire quasi-reference

- (9) Gaunt, A. J.; Scott, B. L.; Neu, M. P. *Inorg. Chem.* **2006**, *45*, 7401.
 (10) Katzin, L. I.; Sonnenberger, D. C. In *The Chemistry of the Actinide Elements*, 2nd ed.; Katz, J. J., Seaborg, G. T., Morss, L. R., Eds.; Chapman & Hall: New York, 1986.
 (11) Clark, A. E.; Martin, R. L.; Hay, P. J.; Green, J. C.; Jantunen, K. C.; Kiplinger, J. L. *J. Phys. Chem. A* **2005**, *109*, 5481.
 (12) Kaltsayannis, N.; Bursten, B. E. *J. Organomet. Chem.* **1997**, *528*, 19.
 (13) Li, J.; Bursten, B. E. *J. Am. Chem. Soc.* **1997**, *119*, 9021.

electrode. Scan rates from 20 to 5000 mV/s were employed to assess the chemical and electrochemical reversibility of the observed redox transformations. Potential calibrations were performed at the end of each data collection cycle using the ferrocenium/ferrocene couple as an internal standard.

Electronic absorption/emission, Raman, and cyclic voltammetric data were analyzed using Wavemetrics IGOR Pro (version 4.0) software on a Macintosh platform or KaleidaGraph (version 3.5) on a Windows platform.

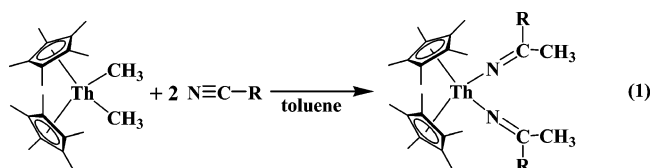
Synthesis. The synthesis of compounds **4–11** is similar to that previously reported for **1–3**. A generic procedure is reported here for complexes **4–11**. For all cases, in an inert atmosphere drybox, toluene solutions of fluorinated nitrile were added dropwise to stirred colorless toluene solutions of $(C_5Me_5)_2Th(CH_3)_2$ contained in a 125-mL flask. The excess nitrile was then rinsed into the reaction using the toluene mixture. Within 30 s of stirring, the reaction mixture turned bright yellow or orange and was stirred at room temperature for 14 h. The volatiles were then removed under reduced pressure, producing an oily residue or solid, which was dissolved in pentane and filtered hot through a Celite-padded coarse frit in all cases. Pure product was obtained either by cooling the concentrated filtrate to $-30\text{ }^\circ\text{C}$ overnight and isolating the crystalline product by decanting the supernatant or by leaving the filtrate to evaporate to dryness at RT for ~ 1 week. The product was further dried under reduced pressure and collected with isolated yields ranging from 44 to 95%. See Supporting Information for additional details.

Computational Methods. Three complexes were selected as representatives to study the fluorine substitution effects by density functional theory: $(C_5Me_5)_2Th[-N=C(Ph)_2]$ (**1**), $(C_5Me_5)_2Th[-N=C(CH_3)(4-F-C_6H_4)]_2$ (**5**), and $(C_5Me_5)_2Th[-N=C(CH_3)(C_6F_5)]_2$ (**11**). The calculations incorporate pentamethylcyclopentadienyl ($C_5Me_5^-$) ligands rather than adopting the computationally simpler strategy of using C_5H_5 as a C_5Me_5 surrogate. The B3LYP hybrid density functional was employed to optimize the equilibrium molecular structures of all complexes.¹⁴ The Stuttgart RSC 1997 effective core potential (ECP) was employed for thorium,¹⁵ where 60 core electrons are replaced to account for scalar relativistic effects. The valence electrons are represented as $[8s/7p/6d/4f]$; 6-31G* basis sets were used for carbon, hydrogen, nitrogen, and fluorine. All calculations were carried out with the *Gaussian03* suite of codes.¹⁶ The excited states were calculated using the time-dependent density functional theory (TD-DFT) approach at optimized ground state geometries.^{17–21} The characterization of excited particle and hole interactions for a given excited state was described by natural transition orbitals (NTOs).²²

Calculations were also performed for the ketimide ligand anions $[-N=C(CH_3)(Ar_F)]^-$. These were modeled after the ketimide ligands found in the corresponding thorium bis(ketimide) complexes. Full geometry optimizations were carried out for the closed shell negative ions of these ligands. Additionally, calculations were performed for lithium and potassium salts of the ketimide anions, but the bare ligand anion results were the most chemically meaningful.

Results and Discussion

Structural Chemistry. Equation 1 displays the synthetic methods used and the yields obtained in the preparation of the fluorinated thorium(IV) ketimide complexes. Treatment of a colorless toluene solution of $(C_5Me_5)_2Th(CH_3)_2$ with 2 equiv of nitrile at room temperature gives the corresponding thorium(IV) bis(ketimide) complexes **4–11** as yellow or orange solids in 44–95% isolated yields. Following workup and crystallization from pentane solution, all complexes were reproducibly isolated in pure form and were characterized by a combination of $^1H/^{13}C/^{19}F$ NMR and UV/vis/NIR absorption and emission spectroscopy, electrochemistry, elemental analysis, and X-ray crystallography. The modest yields for some complexes reflect the high solubility of the bis(ketimide) complexes imparted by the fluorinated ligands.



- R = 3-F-C₆H₄ (**4**), 44 %, orange
 4-F-C₆H₄ (**5**), 48 %, yellow
 2-F-C₆H₄ (**6**), 81 %, yellow
 3,5-F₂-C₆H₃ (**7**), 70 %, orange
 3,4,5-F₃-C₆H₂ (**8**), 48 %, orange
 2,6-F₂-C₆H₃ (**9**), 69 %, yellow
 2,4,6-F₃-C₆H₂ (**10**), 53 %, orange
 C₆F₅ (**11**), 95 %, orange

In contrast to those involving transition metals, synthetic strategies for the preparation of actinide organometallic fluorocarbon complexes are still rare. This has been commonly attributed to the fluorophilicity of the electropositive actinide metal centers, leading to fluoride abstraction chemistry and ultimately preventing more desirable reaction pathways.²³ The system reported here clearly demonstrates that organometallic complexes of actinides containing fluorinated ligands are viable, contrary to the convention that suggests that the strength of An–F bonds would drive their decomposition.^{23–25}

Single-crystal X-ray diffraction studies on **5–11** confirmed their formulation as thorium(IV) bis(ketimide) complexes and were consistent with the NMR data in all cases (Figure 1 and Supporting Information). Experimental crystallographic details are listed in Table 1, while salient geometric parameters are shown in Table 2. Complexes **4–11** display typical bent-metallocene geometries with the ketimide ligands residing within the metallocene wedge. Previous reports of actinide ketimide complexes have stressed the importance of the An–N=C angle and An–N bond distance in discussion of bond order and electronic structure effects. Nitrogen lone pairs on the ketimide ligand have the potential to interact with the metal ion in both σ - and π -modes, resulting in an intermediate An–N bond order between 1 and 2.^{3,4} Interestingly, lanthanide ketimide complexes also exhibit the nearly linear M–N=C angles previously associated with this two-fold metal–ligand interaction in

(14) Becke, A. D. *J. Chem. Phys.* **1993**, *98*, 5648.

(15) Kuchle, W.; Dolg, M.; Stoll, H.; Preuss, H. *J. Chem. Phys.* **1994**, *100*, 7535.

(16) Frisch, M. J.; et al. *Gaussian03*, Revision C.02, Gaussian, Inc.: Wallingford, CT, 2004.

(17) Jamorski, C.; Casida, M. E.; Salahub, D. R. *J. Chem. Phys.* **1996**, *104*, 5134.

(18) Casida, M. E.; Jamorski, C.; Casida, K. C.; Salahub, D. R. *J. Chem. Phys.* **1998**, *108*, 4439.

(19) Bauernschmitt, R.; Ahlrichs, R.; Hennrich, F. H.; Kappes, M. M. *J. Am. Chem. Soc.* **1998**, *120*, 5052.

(20) Stratmann, R. E.; Scuseria, G. E.; Frisch, M. J. *J. Chem. Phys.* **1998**, *109*, 8218.

(21) Petersilka, M.; Gossmann, U. J.; Gross, E. K. U. *Phys. Rev. Lett.* **1996**, *76*, 1212.

(22) Martin, R. L. *J. Chem. Phys.* **2003**, *118*, 4775.

(23) Cuellar, E. A.; Marks, T. J. *Inorg. Chem.* **1981**, *20*, 2129.

(24) Weydert, M.; Andersen, R. A.; Bergman, R. G. *J. Am. Chem. Soc.* **1993**, *115*, 8837.

(25) Dorn, H.; Murphy, E. F.; Shah, S. A. A.; Roesky, H. W. *J. Fluorine Chem.* **1997**, *86*, 121.

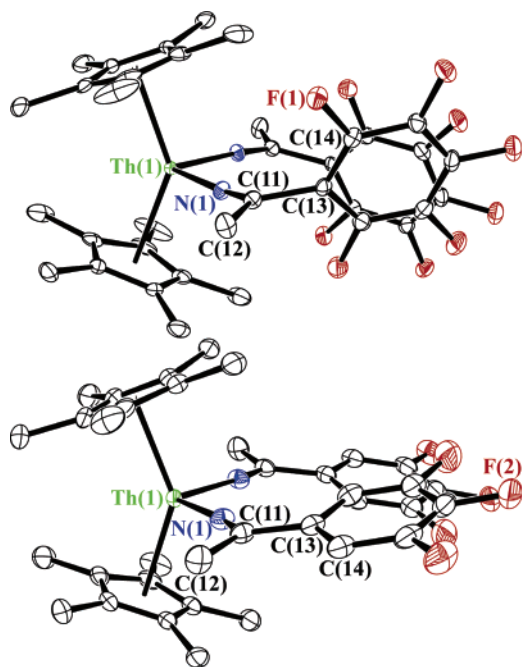


Figure 1. Thermal ellipsoid plots of complexes **11** (top) and **8** (bottom) projected at the 30% probability level. Torsion angles formed by atoms N(1)–C(11)–C(13)–C(14) quantify the relative planarity of the ketimide ligands in **8** and nonplanarity in **11** as a result of the fluorine substitution at the ortho positions.

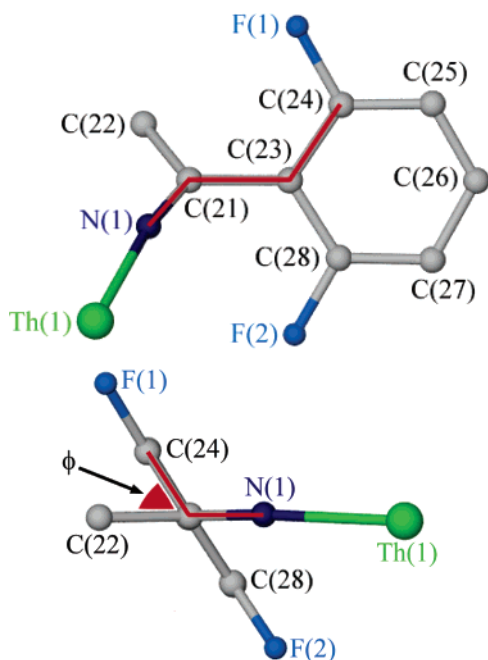


Figure 2. Views orthogonal to (top) and along (bottom) the C(21)–C(23) bond axis of complex **9**. As highlighted in red, the torsion angle N(1)–C(21)–C(23)–C(24) = -121.4° defines the interplanar angle $\phi = 58.6^\circ$. actinide complexes.^{26,27} Given the small radial extension of 4f orbitals and the absence of π -bonding modes in Ln–ketimide complexes, the most important metric for f-element ketimide complexes is decidedly the metal–nitrogen distance.

The Th–N distances in complexes **4–11** are comparable to the values reported for **1** and **2** and show a similar shortening,

falling in between Th(IV)–N amide (2.299(7)–2.398(3) Å) and Th(IV)=N imide (2.045(8) Å) bond distances in structurally related complexes.^{28–32} The Th–N ketimide bonds in complexes **4–11** span the range 2.250(2)–2.286(5) Å. Although the high end of this range begins to approach the Th–N bond distances observed for structurally relevant Th(IV)–amide complexes, overall the Th–N π -bonding interactions in thorium ketimide complexes produce a shortening of ~ 0.1 Å compared to Th–N bond distances in amide systems.

Within the series of complexes, the bond distances and angles do not reveal any particular structural changes that track with changes in their physicochemical properties. Such metrics as the Th–N bond distances are generally within 3σ of each other across the series. The lack of structural and spectroscopic trends (*vide infra*) implies subtlety and competing effects in the global determination of energy states in these complexes; however, electronic structure calculations identified a single primary effect leading to the observed geometries of the complexes. Fluorine substitution at the ortho position on the ketimide aryl group imposes an unfavorable steric demand that forces the aryl group to be rotated orthogonal to planes formed by the corresponding ketimide N=C(C_{Me})(C_{ipso}) atoms. This out-of-plane rotation can be observed by comparing the molecular structures for complexes **11** and **8** in Figure 1. As demonstrated in Figure 2, the amount of rotation can be quantified by analyzing the torsion angles that describe the smallest interplanar angle formed by atoms N(1)–C(21)–C(23)–C(24/28). Looking down the C(21)–C(23) axis, out-of-plane distortions of the aryl ring result from either clockwise or counterclockwise rotation of the group along the C(21)–C(23) axis. The interplanar angles (ϕ) range from 0° (aryl groups planar to ketimide atoms N=C(C_{Me})(C_{ipso})) to 90° (orthogonal aryl groups). As shown in Table 2, two distinct structure types emerge from this analysis: complexes **5**, **7**, and **8** exhibit interplanar angles in the range $\phi = 5.7$ – 34.9° while **6**, with its single site of ortho-fluorination, has $\phi = 24.7$ and 48.0° . Compounds **9–11** exhibit significantly larger values in the range $\phi = 49.1$ – 88.8° .

The structure of **7** and one of the two molecules in the asymmetric unit of **9** display an additional type of distortion in which a ketimide ligand is rotated nearly 180° around its Th–N bond axis such that the ketimide methyl group points approximately “inward” toward the aryl group of the second ketimide ligand (see Supporting Information). Because both of these rotational conformations are present in the structure of **9**, this suggests that a low rotational energy barrier exists for the ketimide ligand, which is consistent with the ambient-temperature NMR spectroscopy data. The observation of this rotational variation in the structures of **7** and **9** is presumably due to crystal packing forces; the rotational conformers adhere to the ketimide–aryl group planarity/nonplanarity described above. In total, the structural data imply an overall destabilization in compounds **9–11** due to disruption of conjugation of the fluorinated aromatic groups with the aza-vinyl moieties in the ketimide ligands.

(26) Evans, W. J.; Forrestal, K. J.; Ziller, J. W. *J. Am. Chem. Soc.* **1998**, *120*, 9273.

(27) Hou, Z. M.; Yoda, C.; Koizumi, T.; Nishiura, M.; Wakatsuki, Y.; Fukuzawa, S.; Takats, J. *Organometallics* **2003**, *22*, 3586.

(28) Gilbert, T. M.; Ryan, R. R.; Sattelberger, A. P. *Organometallics* **1988**, *7*, 2514.

(29) Barnhart, D. M.; Clark, D. L.; Grumbine, S. K.; Watkin, J. G. *Inorg. Chem.* **1995**, *34*, 1695.

(30) Korobkov, I.; Gambarotta, S.; Yap, G. P. A. *Angew. Chem., Int. Ed.* **2003**, *42*, 814.

(31) Haskel, A.; Straub, T.; Eisen, M. S. *Organometallics* **1996**, *15*, 3773.

(32) Straub, T.; Haskel, A.; Neyroud, T. G.; Kapon, M.; Botoshansky, M.; Eisen, M. S. *Organometallics* **2001**, *20*, 5017.

Table 1. Crystallographic Experimental Parameters for 5–11

	5	6	7	8	9	10	11
formula	C ₃₆ H ₄₄ F ₂ N ₂ Th	C ₃₆ H ₄₄ F ₂ N ₂ Th	C ₃₆ H ₄₂ F ₄ N ₂ Th	C ₃₆ H ₄₀ F ₆ N ₂ Th	C ₃₆ H ₄₂ F ₄ N ₂ Th	C ₃₆ H ₄₀ F ₆ N ₂ Th	C ₃₆ H ₃₆ F ₁₀ N ₂ Th
<i>a</i> (Å)	12.9201(6)	10.180(5)	15.568(2)	13.087(3)	10.7290(5)	14.566(2)	16.066(3)
<i>b</i> (Å)	14.0054(7)	17.880(8)	11.3893(17)	13.927(3)	17.7108(8)	16.206(2)	16.393(3)
<i>c</i> (Å)	18.2113(9)	18.364(8)	18.841(3)	18.783(5)	19.3565(9)	15.119(2)	26.997(5)
α (deg)	90	90	90	90	108.7590(10)	90	90
β (deg)	98.677(1)	90	90.668(3)	99.272(3)	90.1920(10)	94.027(2)	90
γ (deg)	90	90	90	90	102.9020(10)	90	90
<i>V</i> (Å ³)	3257.6(3)	3343(3)	3340.3(9)	3378.7(14)	3383.5(3)	3560.1(8)	7110(2)
<i>Z</i>	4	4	4	4	4	4	8
FW	774.77	774.77	810.76	846.74	810.76	846.74	918.71
space group	<i>C2/c</i>	<i>P2₁2₁2₁</i>	<i>P2₁/c</i>	<i>P2₁/c</i>	<i>P1</i>	<i>C2/c</i>	<i>Pccn</i>
<i>T</i> (K)	141(2)	203(2)	203(2)	141(1)	141(2)	203(2)	141(2)
λ (Å)	0.71073	0.71073	0.71073	0.71073	0.71073	0.71073	0.71073
<i>D</i> _{calc} (g·cm ⁻³)	1.580	1.540	1.612	1.665	1.592	1.580	1.717
μ (mm ⁻¹)	4.615	4.498	4.513	4.474	4.455	4.246	4.275
<i>R</i> 1 (<i>I</i> > 2 σ (<i>I</i>))	0.0204	0.0359	0.0413	0.0145	0.0442	0.0309	0.0249
w <i>R</i> 2 (all data)	0.0578	0.0794	0.0860	0.0372	0.1092	0.0790	0.0594

Table 2. Selected Metrical Parameters for Complexes 1, 2, and 5–11 from X-ray Diffraction Data

	1	2	5	6	7	8	9	10	11
Th–N (Å)	2.259(4) 2.265(5)	2.256(8)	2.250(2)	2.260(5) 2.269(5)	2.263(5) 2.286(5)	2.2727(19)	2.255(5) 2.261(5) 2.255(5) 2.263(5)	2.263(3)	2.268(3) 2.273(3)
N=C (Å)	1.259(7) 1.272(7)	1.264(13)	1.259(4)	1.265(8) 1.248(8)	1.245(7) 1.268(7)	1.256(3)	1.272(8) 1.280(8) 1.262(8) 1.273(8)	1.253(5)	1.253(4) 1.251(4)
Th–N=C (deg)	174.0(4) 179.4(5)	161.2(8)	175.5(2)	176.6(5) 174.7(5)	172.8(4) 170.8(4)	170.5(2)	171.4(5) 177.1(5) 171.9(5) 167.3(5)	174.7(4)	176.0(2) 177.1(2)
N–Th–N (deg)	108.95(17)	102.9(4)	108.83(13)	108.65(19)	107.37(17)	109.72(11)	107.35(19) 104.8(2)	108.2(2)	105.96(13) 104.90(13)
ϕ (deg) ^a			8.4	24.7 48.0	34.9 27.7	5.7	56.2 88.8 49.1 57.7	72.4	68.5 75.6

^a See Figure 2 for definition.

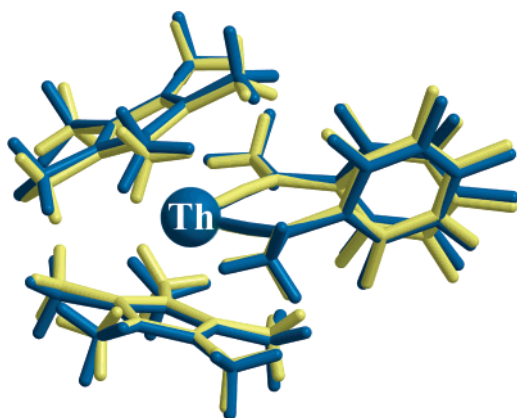


Figure 3. Overlapping atomic coordinates obtained from DFT optimized ground-state structure (blue) and the experimental crystal structure (yellow) for complex **11**. The representation demonstrates the excellent agreement between calculated and observed ground-state geometries for this complex.

Computational Studies. The structures of the ground states for the three thorium bis(ketimide) complexes (C₅Me₅)₂Th[–N=C(Ph)₂]₂ (**1**), (C₅Me₅)₂Th[–N=C(CH₃)(4-F-C₆H₄)]₂ (**5**), and (C₅Me₅)₂Th[–N=C(CH₃)(C₆F₅)]₂ (**11**) were calculated using DFT approaches. Figure 3 shows overlapping projections of the atomic coordinates obtained from the DFT optimized ground-

state structure and data obtained from the crystal structure for **11**. Excellent agreement is obtained between the experimental and calculated structures as shown in Figure 3. For complexes **5** and **11**, the most significant difference in the optimized structures is the orientation of the ketimide aryl ring; it lies in the N=C(C_{Me})(C_{ipso}) plane for complex **5**, while it is rotated out of the plane ($\phi = 67.7^\circ$ calc versus 75.6 and 68.5° expt) for complex **11**. As discussed in detail below, this appears to arise principally from unfavorable steric interactions between the ortho fluorine atoms on the aryl ring and the ketimide ligand methyl group [–N=C(CH₃)]. Finally, in the optimized structure for complex **1**, one phenyl ring lies in this plane, while unfavorable steric interactions rotate the second phenyl ring out of the plane.

In terms of the canonical molecular orbitals derived from the ground-state properties, several observations can be made regarding the highest occupied molecular orbitals (HOMOs). In addition to the two orbitals that are predominantly nitrogen lone pair in character, there are four other orbitals in the same energy region arising from the π -systems of the pentamethylcyclopentadienyl (C₅Me₅) ligands. These comprise the two pairs of degenerate π -orbitals that are the HOMOs in the two isolated pentamethylcyclopentadienyl ligands. Overall, the set of six orbitals have energies differing by only 0.8 eV (0.03 au) as

Table 3. Mulliken Analysis of the Contributions (%) to the Molecular Orbitals in Complexes **5** and **11**

orbital	E (au)	Th			C=N		Ar _F	C ₅ Me ₅
		sp	d	f	N	C		
(C ₅ Me ₅) ₂ Th[−N=C(CH ₃)(4-F-C ₆ H ₄)] ₂ (5)								
LUMO+1	−0.045	3.1	8.8	18.2	16.4	29.8	17.4	2.8
LUMO	−0.050	0.0	9.3	21.6	14	29.2	14.8	7.6
HOMO	−0.187	0.3	0.1	9.1	33.8	1.4	6.0	46.0
HOMO−1	−0.192	4.8	4.0	0.6	25.2	1.0	3.8	56.6
HOMO−2	−0.193	4.3	2.2	3.5	29.7	1.4	7.4	48.2
HOMO−3	−0.202	0.4	9.0	4.0	3.2	1.4	0.6	80.9
HOMO−4	−0.203	0.1	11.4	1.9	6.8	2.6	5.0	70.9
HOMO−5	−0.217	0.0	17.2	0.7	28.5	1.6	7.0	41.1
(C ₅ Me ₅) ₂ Th[−N=C(CH ₃)(C ₆ F ₅)] ₂ (11)								
LUMO+1	−0.043	2.2	6.0	12.1	16.4	24.0	34.2	1.8
LUMO	−0.049	0.0	6.7	14.9	14.4	24.2	31.2	5.4
HOMO	−0.193	2.1	0.5	5.7	5.8	0.2	0.4	84.3
HOMO−1	−0.198	4.5	3.5	0.8	13.2	0.6	1.2	74.1
HOMO−2	−0.206	1.4	4.7	5.7	29.6	1.8	6.0	47.6
HOMO−3	−0.211	1.5	6.7	4.9	33.2	1.8	4.8	43.2
HOMO−4	−0.213	0.0	12.5	1.8	1.6	2.8	0.8	79.4
HOMO−5	−0.225	0.2	17.6	0.7	48.4	1.8	8.8	16.6

shown in Table 3. For (C₅Me₅)₂Th[−N=C(CH₃)(4-F-C₆H₄)]₂ (**5**), there is much more nitrogen character in the HOMO (33.8%), while in (C₅Me₅)₂Th[−N=C(CH₃)(C₆F₅)]₂ (**11**) the HOMO has only 5.8% nitrogen character. In contrast, there is only 46% contribution from the C₅Me₅ ligands to the HOMO in complex **5** versus 84% in **11**. The lowest two unoccupied orbitals (LUMOs) predominantly consist of the N=C and aryl ring π* orbitals with small contributions from thorium 6d- and 5f-orbitals. For (C₅Me₅)₂Th[−N=C(CH₃)(4-F-C₆H₄)]₂ (**5**), this latter contribution (9% 6d and 18–22% 5f) is larger than that found in (C₅Me₅)₂Th[−N=C(CH₃)(C₆F₅)]₂ (**11**) (6% 6d and 12–15% 5f).

To assess the role of fluorine substitution on the ketimide aryl groups and the impact of the sterically induced structural distortion on the energies of the electronic states, TD-DFT studies were performed on complexes **1**, **5**, and **11** for comparison with spectroscopic results discussed below. The calculated excited-state energies from TD-DFT calculations at the optimized ground-state geometries are summarized in Table 4. There is a pair of nearly degenerate singlet states for each molecule (for example, 2.69 (S₁) and 2.76 eV (S₂) for complex **5**). In addition, the calculated S₁ excitation energies quantitatively mirror the experimental increase (vide infra) as one goes along the series of three complexes: complex **1**, 2.56 eV calc versus 2.48 eV expt; complex **5**, 2.69 eV calc versus 2.62 eV expt; complex **11**, 3.03 eV calc versus 2.96 eV expt. We also note that the predicted S₁ and S₂ states for the model complex Cp₂Th[−N=C(Ph)₂]₂ (**1a**)¹¹ were uniformly higher by only 0.13

eV compared to (C₅Me₅)₂Th[−N=C(Ph)₂]₂ (**1**). Similarly, a very small deviation (0.04 eV) of the calculated singlet excitation energies is observed between (C₅Me₅)₂Th[−N=C(CH₃)(4-F-C₆H₄)]₂ (**5**) and its model complex Cp₂Th[−N=C(CH₃)(4-F-C₆H₄)]₂ (**5a**).

As noted, both S₁ and S₂ states arise from promotion of an electron from a nonbonding nitrogen p orbital to an antibonding C=N π* orbital (p_N→π*_{C=N}).¹¹ While this is less evident from the MO parentages in the TD-DFT calculation where each state has four to six major contributions, it becomes more easily visualized when viewed in terms of natural transition orbitals (NTO), which give the most compact particle–hole description of each state.²² For complex **1**, this S₁ representation collapses to a single excitation involving an occupied “hole” orbital (H) with predominantly nitrogen character and a virtual “particle” (P) orbital involving the π-systems of the ketimide (C=N) and aryl groups, both localized on a single ketimide ligand. The corresponding S₂ state involves a similar excitation on the second ketimide ligand. This result is very similar to earlier calculations on the model complex **1a**.¹¹ For complexes **5** and **11**, a parallel picture emerges with the exception that the particle and hole orbitals are delocalized over both ketimide ligands (Table 5). In contrast to **1** and **1a**, complexes **5** and **11** possess a mirror plane of symmetry that passes between the two ketimide ligands, and the particle and hole orbitals are either symmetric (S) or antisymmetric (A) with respect to this mirror plane. For the S₁ states, the combination involves occupied to virtual orbital A→A excitations in both complexes **5** and **11**. However, for the S₂ states, the combination involves an occupied to virtual orbital A→S excitation for **5** and S→A excitation for **11**. These lowest excited states are mainly localized on the ketimide ligands with small contributions from pentamethylcyclopentadienyl ligands rings based on the NTO representations. As a consequence, the experimental spectroscopic data for the complexes are expected to show some significant variability for the different ketimide ligands.³³

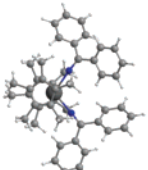
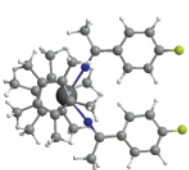
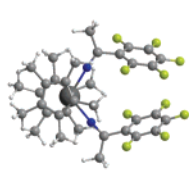
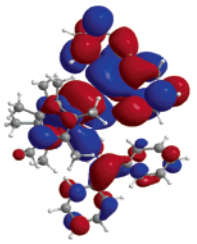
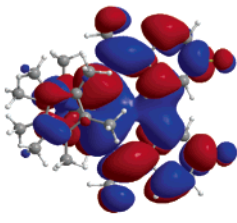
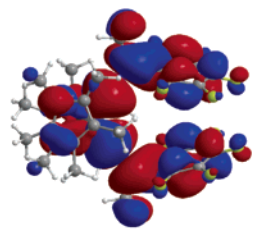
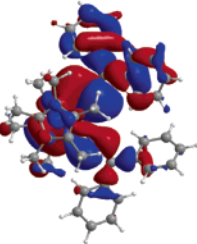
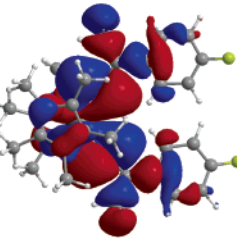
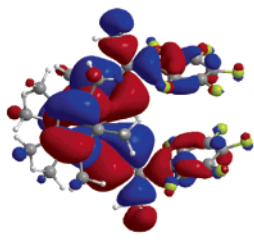
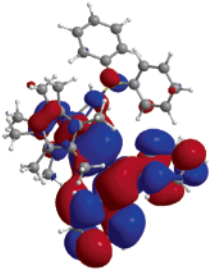
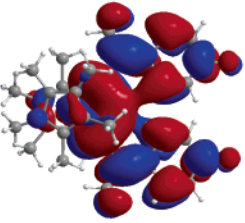
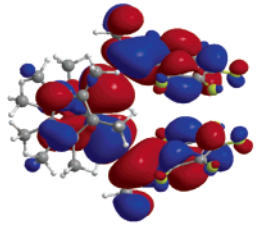
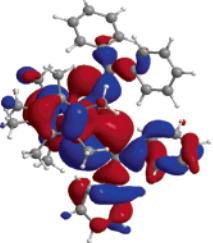
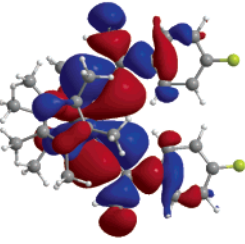
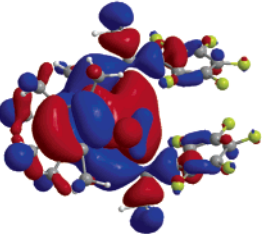
In order to better understand the overall trends in the excitation energies of the fluorinated bis(ketimide) complexes **4–11**, the excited states of isolated ketimide ligands were also systematically examined using DFT techniques. In lieu of time-intensive excited-state calculations on all the complexes in the series, isolated ketimide ligand calculations were performed to obtain direct information on the S₁ energies for comparison without perturbation from metal-based orbitals. The closed shell negative ions of the ligands, [−N=C(CH₃)(Ar_F)][−], were chosen as the most chemically meaningful set for this purpose, after examining other alternatives such as alkali metal–ligand compounds. The results are displayed in Figure 4, where the

Table 4. Excitation Energies from TD-DFT Calculations for Complexes **1**, **1a**, **5**, **5a**, and **11**

	expt ^a	calc	calc
			(C ₅ H ₅) ₂ Th[−N=C(Ph) ₂] ₂ (1a)
S1	2.48	2.56	2.69 ^b
S2	2.64	2.61	2.75 ^b
			(C ₅ Me ₅) ₂ Th[−N=C(CH ₃)(4-F-C ₆ H ₄)] ₂ (5)
S1	2.62	2.69	2.65
S2	2.85	2.76	2.79
			(C ₅ Me ₅) ₂ Th[−N=C(CH ₃)(C ₆ F ₅)] ₂ (11)
S1	2.96	3.03	—
S2	2.97	3.05	—

^a From Gaussian fits of ambient temperature electronic absorption spectral data. ^bSee text.

Table 5. Singlet Natural Transition Orbitals for Complexes 1, 5, and 11

	Complex 1	Complex 5	Complex 11
			
	2.56 eV	2.69 eV	3.03 eV
S1	P 		
	H 		
	2.61 eV	2.76 eV	3.05 eV
S2	P 		
	H 		

calculated $S_1(L)$ excited-state energy of the $[-N=C(CH_3)(Ar_F)]^-$ ligand at the optimized ground-state geometry is compared with that of the average energy of the S_1 and S_2 transitions [$S_{ave}(expt)$] from the corresponding thorium bis(ketimide) complex absorption spectroscopy data. The results are presented with the $[-N=C(CH_3)(Ar_F)]^-$ ligands in order of roughly increasing $S_{ave}(expt)$ energy for the corresponding thorium bis(ketimide) complexes.

The overall trend for the thorium complexes of increasing excitation energy is also qualitatively followed for the free $[-N=C(CH_3)(Ar_F)]^-$ ketimide ligands, with the $S_1(L)$ energy

of $[-N=C(CH_3)(2,4,6-F_3-C_6H_2)]^-$ lying somewhat lower compared to the energies of the rest of the series. The biggest difference arises for the three ketimide ligands $[-N=C(CH_3)(2,6-F_2-C_6H_3)]^-$, $[-N=C(CH_3)(2,4,6-F_3-C_6H_2)]^-$, and $[-N=C(CH_3)(C_6F_5)]^-$ where there is an unfavorable steric interaction between one of the two ortho fluorine atoms and the ketimide moiety $[-N=C(CH_3)]$. In these three structures the fluorinated aryl ring is rotated out of the $N=C(C_{Me})(C_{ipso})$ plane to accommodate this repulsive interaction (see Supporting Information for pictorial representations). As a result of these nonplanar ligand structures, the conjugation of the π -orbitals is

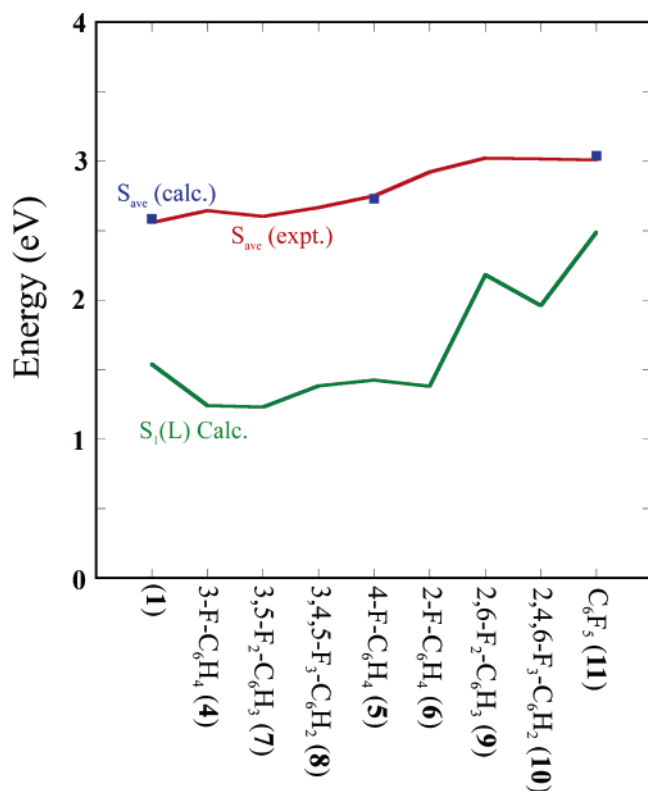


Figure 4. Comparison of DFT calculated transition energies for ketimide ligand anions (green line), $(C_5Me_5)_2Th[-N=C(Ph)_2]_2$ (1) and select $(C_5Me_5)_2Th[-N=C(CH_3)(Ar_F)]_2$ complexes (blue points), and averaged experimental electronic absorption data for the two, nearly degenerate transitions S_1 and S_2 (red line).

also disrupted in the corresponding three thorium complexes (9–11). In the case of a single ortho fluorine substituent, the ground-state structure for $[-N=C(CH_3)(2-F-C_6H_4)]^-$ adopts a planar arrangement with the aryl group rotated such that the F- C_{Ar} carbon atom is *trans* to the ketimide nitrogen atom with respect to the NC- C_{ipso} bond.

Electrochemistry. Typical cyclic voltammograms for the thorium bis(ketimide) complexes in 0.1 M $[Bu_4N][B(C_6F_5)_4]/THF$ are shown in Figure 5. Redox potential data for all complexes are provided in Table 6. As shown in Figure 5 and noted in previous studies, the principal redox activity is limited to reduction processes that take place at potentials near the negative limit of this supporting electrolyte/solvent system.^{3b} These processes have been ascribed to ketimide ligand-based reductions because nearly identical reduction waves are observed in the analogous uranium bis(ketimide) complexes and because metal-based reduction of the closed-shell Th(IV) ion is expected to lie to much more negative potentials than could be accessed under these experimental conditions. The characteristics of the voltammetric waves are for the most part consistent with irreversible electron-transfer steps, although there is a wide range of observed behavior as reflected in the traces shown in Figure 5. In addition, coupled chemical processes are observed in most cases as revealed by the appearance of new anodic peaks in the potential region from ~ -0.5 to -2.0 V that are not observed if the potential is first scanned in the positive direction (Figure 5).

It is noteworthy that many complexes exhibit two discrete reduction waves that are separated by ~ 100 – 400 mV (Table 6). This behavior is attributed to the sequential addition of an

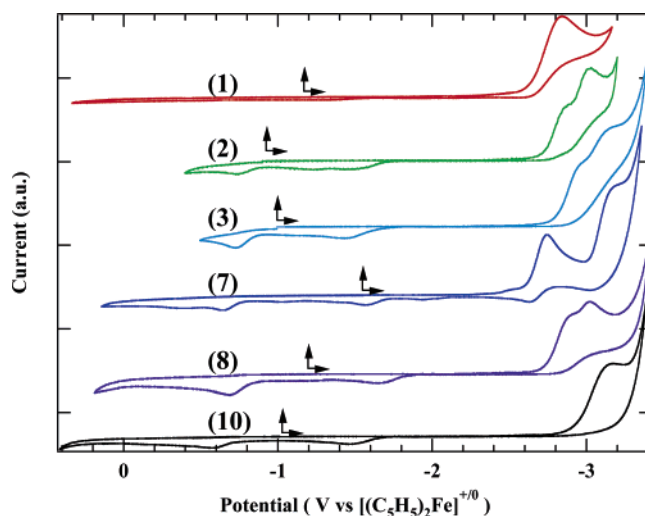


Figure 5. Cyclic voltammetric data for ~ 5 mM $(C_5Me_5)_2Th[-N=C(R_1)(R_2)]_2$ (where $R_1, R_2 = Ph$ (1); $R_1 = Ph, R_2 = CH_2Ph$ (2); $R_1 = Ph, R_2 = CH_3$ (3); $R_1 = CH_3, R_2 = 3,5-F_2-C_6H_3$ (7); $R_1 = CH_3, R_2 = 3,4,5-F_3-C_6H_2$ (8); $R_1 = CH_3, R_2 = 2,4,6-F_3-C_6H_2$ (10)) in ~ 0.1 M $[Bu_4N][B(C_6F_5)_4]/THF$ at room temperature. All scans were collected at 200 mV/s. Vertical arrows indicate the rest (initial) potential for the scans and the horizontal arrows indicate the initial scan direction.

electron into each of two nearly degenerate ketimide-based orbitals consistent with the theoretical results for the LUMOs described above. The apparent absence of multiple reduction waves in some of these thorium bis(ketimide) complexes is likely a reflection of close spacing of multiple waves that precludes resolution of discrete waves in the voltammetry and/or the proximity of these processes to the negative potential limit in this supporting electrolyte/solvent system that prohibits observation of analyte behavior. In general, this electrochemical behavior parallels the spectroscopic data described in detail below, indicating that there are two discrete, nondegenerate, low-lying virtual orbitals ($\Delta E \approx 0.1$ eV) available to accept the added electrons.

Electronic Absorption Spectroscopy. As noted in previous investigations the unusual intense color of the thorium bis(ketimide) complexes in the solid state and in solution derives from the existence of a moderately intense, broad electronic transition in the mid-visible spectral region.^{3,11} The electronic spectral data for complexes 1–11 are shown in Figure 6. Clearly all 11 complexes exhibit this same hallmark spectral feature, although the energy and intensity varies significantly across the series, reflecting electronic perturbation by the fluorinated aryl substituents. TD-DFT calculations have predicted this significant variability across the ketimide derivatives with the lowest-energy electronic absorption spectral features in the thorium bis(ketimide) complexes derived from transitions best described as $p_N \rightarrow \pi^*_{C=N}$, with two nearly degenerate transitions (S_1 and S_2) of this description. In fact, all the spectra shown in Figure 6 can be quite adequately fit using a sum of three Gaussian bands; one for the unresolved very high-energy feature and two for the mid-visible features under discussion here. The two-band model for this mid-visible feature is a necessary and sufficient condition for fitting of all 11 spectra and is consistent with the TD-DFT calculations. Examples of the resultant fits

(33) The preceding discussion refers to the dominant component of the NTO analysis for a given state. Additional details are given in the Supporting Information.

Table 6. Summary of Physical Chemical Data for the Thorium Bis(ketimide) Complexes, $(C_5Me_5)_2Th[-N=C(R_1)(R_2)]_2$

complex	reduction potentials (V vs $[(C_5H_5)_2Fe]^{+/0}$)		room-temperature electronic absorption data ^a							77 K electronic emission data ^b		
			high-energy band		low-energy band			$\Sigma(\text{osc. strength})$ ($\times 10^3$)	$E_{00}(S_1)$ (cm^{-1})	$E_{00}(T_1)$ (cm^{-1})	τ_{meas} (μs)	
			E_{max} (cm^{-1})	osc. strength ^c ($\times 10^3$)	E_{max} (cm^{-1})	osc. strength ^c ($\times 10^3$)						
R_1	R_2	$E_{1/2}(1)$	$E_{1/2}(2)$									
1	Ph	Ph	-2.78	^d	21310	5.9	19900	1.6	7.5	19900	16460	50
2	Ph	CH ₂ Ph	-2.84	-2.99	23030	0.3	21620	1.8	2.1	20380	18130	410
3	Ph	CH ₃	-2.94	-3.12	22830	0.9	21170	1.0	1.9	22100	18330	400
4	CH ₃	3-F-C ₆ H ₄	-2.90	-2.99	22160	2.1	20480	0.5	2.6	22110	19100	340
5	CH ₃	4-F-C ₆ H ₄	-2.53	^d	22890	3.0	21180	1.1	4.1	21800	19600	140
6	CH ₃	2-F-C ₆ H ₄	-2.99	-3.08	24620	5.4	22520	5.1	10.5	21440	18290	400
7	CH ₃	3,5-F ₂ -C ₆ H ₃	-2.70	-3.11	21830	3.3	20170	0.6	3.9	20500	18660	290
8	CH ₃	3,4,5-F ₃ -C ₆ H ₂	-2.83	-2.92	22340	2.5	20700	1.5	4.0	20640	18760	290
9	CH ₃	2,6-F ₂ -C ₆ H ₃	-2.94	^d	25350	1.8	23410	6.9	8.7	20760	18440	350
10	CH ₃	2,4,6-F ₃ -C ₆ H ₂	-3.08	^d	25240	1.7	23440	5.8	7.5	22850	18700	290
11	CH ₃	C ₆ F ₅	-2.84	-3.02	23950	1.8	23840	6.6	8.4	^d	18150	360

^a Metrical parameters derived from Gaussian fits. See text for details. ^b E_{00} values estimated from apparent position of highest energy vibronic component. ^c Calculated from spectral fit data according to Eqn. 4.2 in ref 34. ^d Not observed.

to these putative $n\pi^*$ transitions are illustrated in Figure 6 for complexes **1** and **5**. The metrical data derived from these fits are compiled in Table 6. Note that the oscillator strengths³⁴ in these transitions ($\sim 10^{-3}$) are wholly consistent with their assignments, being spin-allowed but orbitally forbidden in character, and agree well with previously reported TD-DFT calculations.¹¹

The assignment of the lowest excited states to ketimide-localized $n\pi^*$ transitions is also supported by experimental observations and theoretical calculations for the structurally and electronically analogous $Cp_2Zr[-N=C(Ph)_2]_2$ (**12**) for which a very similar mid-visible spectral feature is observed.^{5,11} In fact, 77 K electronic absorption spectral data for both $Cp_2Zr[-N=C(Ph)_2]_2$ (**12**) and $(C_5Me_5)_2Th[-N=C(Ph)_2]_2$ (**1**) clearly show vibronic resolution in this lowest-energy absorption feature (see Supporting Information) as might be expected for an $n\pi^*$ transition in which there is a net change in the ketimide ligand bonding between the ground and excited states. The observed vibronic progressions ($\sim 1300\text{ cm}^{-1}$ for **12**; $\sim 1200\text{ cm}^{-1}$ for **1**) do not correspond to real vibrational modes in these systems; this is the familiar “MIME” effect in systems having multiple Franck–Condon active vibrational modes.^{35–37} However, the observation of this resolved vibronic structure entailing several Franck–Condon active modes in the absorption spectra suggests (1) that the structural distortions in these excited states are not simply localized on the C=N fragment and (2) that these thorium ketimide systems are poised to yield resonance-enhanced Raman spectra discussed below.⁵

Finally, the trend in the energies of these two singlet $n\pi^*$ transitions across the series of ketimide ligands is wholly consistent with predictions from the TD-DFT calculations described above for the entire series of anionic ketimide free ligands and for the three complexes for which full calculations were carried out (Figure 4). Of particular note is the apparent influence of the sterically induced structural distortion in complexes **9–11**. As illustrated in Figure 4, the average value for the two singlet $n\pi^*$ transitions for all three of these distorted complexes is significantly greater than that for all other

complexes for which no substantial structural distortion is observed. This is a clear manifestation of the disruption of the π^* orbital network across the $-N=C(CH_3)(Ar_F)$ framework that has the net effect of raising the energy of the terminal π^* orbital in the $n\pi^*$ transition.

Electronic Emission Spectroscopy. Perhaps the most interesting aspect of the spectroscopic properties of these thorium bis(ketimide) complexes is that they exhibit luminescence. The emission was first observed in the course of surveying their Raman spectral behavior using blue laser excitation in which the emission, even at room temperature, could be clearly seen emanating from the laser excitation volume. Subsequent, more detailed studies confirmed that this luminescent behavior is generic to all the thorium bis(ketimide) complexes reported here; it is quite intense and long-lived at 77 K for all complexes, the range of energies parallels that seen in the electronic absorption data, and the decay pathways are both surprising and complex, particularly in light of the presence of such a high Z metal in intimate proximity with the emitting chromophore. Indeed, while luminescence is fairly common in d^0 transition-metal complexes, including $Cp_2Zr[-N=C(Ph)_2]_2$ (**12**) (see Supporting Information), it is typically ligand-to-metal charge transfer in nature as observed in systems like $Cp_2Ti(NCS)_2$.^{38–43} There appear to be only a few examples of Th(IV) systems for which optical emission has been reported, and most of these examples are based on porphyrin-type complexes for which the emission is also ligand-based.^{44–48} However, it has been pointed out that high Z metals like Th can actually be used to induce preferential phosphorescence decay over fluorescence in organic ligands as a result of enhanced spin–orbit coupling.⁴⁶

- (34) Lever, A. B. P. *Inorganic Electronic Structure and Spectroscopy*, 2nd ed.; Elsevier: Amsterdam, 1984.
 (35) Tutt, L.; Tannor, D.; Schindler, J.; Heller, E. J.; Zink, J. I. *J. Phys. Chem.* **1983**, *87*, 3017.
 (36) Tutt, L. W.; Zink, J. I.; Heller, E. J. *Inorg. Chem.* **1987**, *26*, 2158.
 (37) Tutt, L.; Tannor, D.; Heller, E. J.; Zink, J. I. *Inorg. Chem.* **1982**, *21*, 3858.

- (38) Pfenning, B. W.; Thompson, M. E.; Bocarsly, A. B. *Organometallics* **1993**, *12*, 649.
 (39) Patrick, E. L.; Ray, C. J.; Meyer, G. D.; Ortiz, T. P.; Marshall, J. A.; Brozik, J. A.; Summers, M. A.; Kenney, J. W. *J. Am. Chem. Soc.* **2003**, *125*, 5461.
 (40) Tonzetich, Z. J.; Eisenberg, R. *Inorg. Chim. Acta* **2003**, *345*, 340.
 (41) Yam, V. W. W.; Qi, G. Z.; Cheung, K. K. *Organomet. Chem.* **1997**, *548*, 289.
 (42) Yam, V. W. W.; Qi, G. Z.; Cheung, K. K. *Organometallics* **1998**, *17*, 5448.
 (43) Yam, V. W. W.; Qi, G. Z.; Cheung, K. K. *J. Chem. Soc., Dalton Trans.* **1998**, 1819.
 (44) Bilsel, O.; Rodriguez, J.; Milan, S. N.; Gorlin, P. A.; Girolami, G. S.; Suslick, K. S.; Holten, D. *J. Am. Chem. Soc.* **1992**, *114*, 6528.
 (45) Knor, G.; Strasser, A. *Inorg. Chem. Commun.* **2002**, *5*, 993.
 (46) Kunkely, H.; Vogler, A. *Chem. Phys. Lett.* **1999**, *304*, 187.
 (47) Martarano, L. A.; Wong, C. P.; Horrocks, W. D.; Goncalves, M. P. *J. Phys. Chem.* **1976**, *80*, 2389.
 (48) Tranthi, T. H.; Dormond, A.; Guillard, R. *J. Phys. Chem.* **1992**, *96*, 3139.

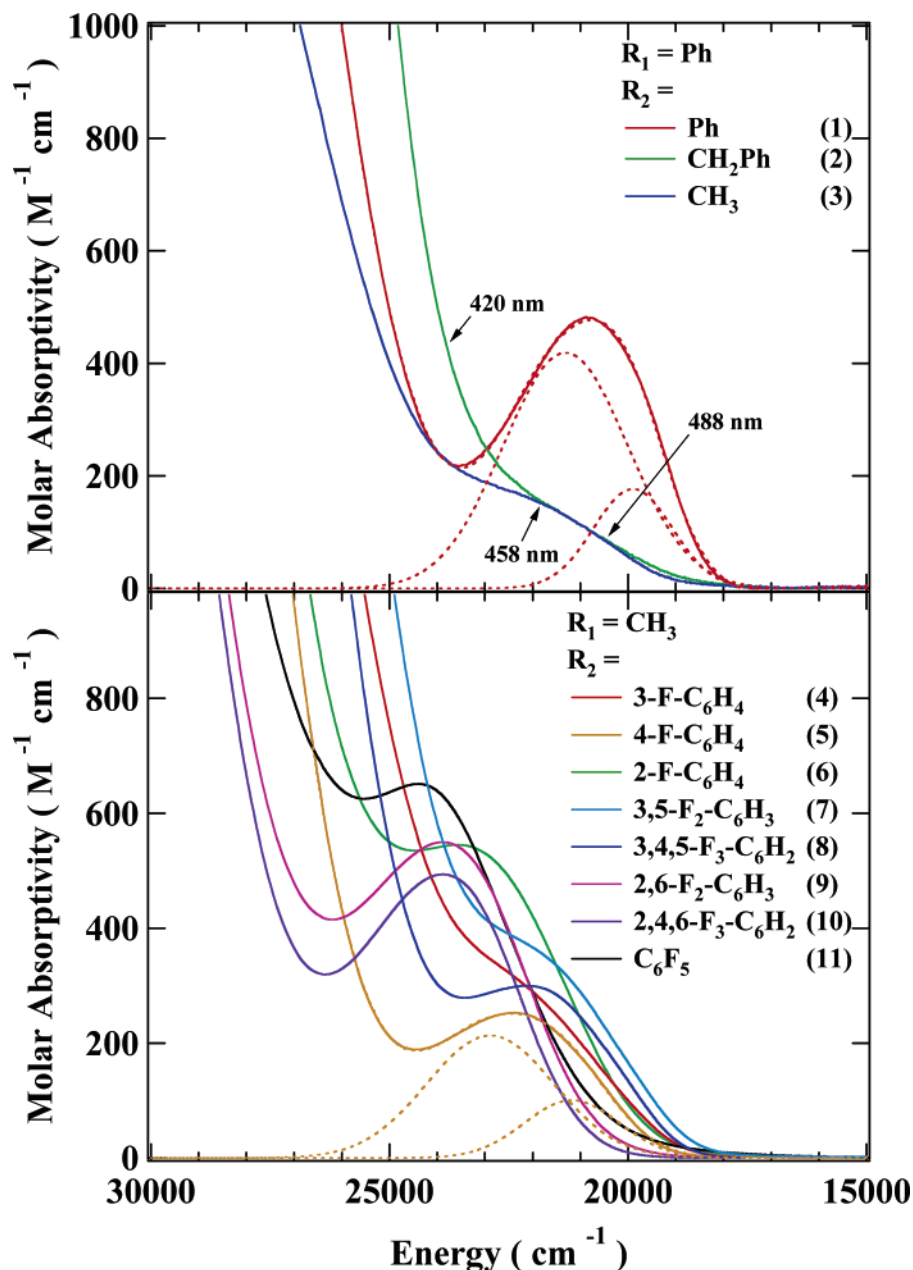


Figure 6. UV–visible electronic absorption spectra for $(C_5Me_5)_2Th[-N=C(R_1)(R_2)]_2$ in toluene solution at room temperature. Spectral deconvolutions of the constituent bands in the low-energy region are shown in dashed lines for **1** and **5**. Wavelength markers in top panel denote excitation wavelengths used for Raman spectra of **2**, shown in Figure 9.

Typical 77 K emission and emission excitation data are illustrated in Figure 7 for complexes **1** and **5**. The room-temperature electronic absorption spectral data are superimposed on these emission results, and the correspondence in energy of the low-lying $n\pi^*$ absorption transitions described above with the manifold of emission bands suggests that the luminescence originates from these same ketimide ligand-localized states. Note, however, that the emission spectral behavior in particular is inconsistent with a simple organic fluorescent-like behavior. The substantial shift ($\sim 4000\text{ cm}^{-1}$) observed between the emission maximum and the excitation maximum in the data for **1** is more in keeping with emission from a relaxed triplet state following excitation into the singlet manifold. The more surprising result is the appearance of distinct multiple emission bands in the case of complex **5** as seen from the emission spectrum obtained using CW excitation (Figure 7, bottom, green

trace). The contribution of this higher-energy band to the total emission envelope disappears under time-resolved excitation/detection conditions (red trace), demonstrating that the lifetime of this state is much less than that of the lower-lying, longer-lived state. This multiple-state emission behavior is a common feature of all complexes reported here except for **1** and **11**.

There are several different scenarios that can give rise to multiple-state emission behavior. The two most common are (1) spatially isolated emission in which the emissive states are localized in spatially distinct, electronically uncoupled (or very weakly coupled) orbitals on the molecule^{49,50} and (2) singlet and triplet emission from states having a common orbital parentage.⁴⁵ We believe the latter is the more precise description of the operative mechanism in the thorium bis(ketimide)

(49) DeArmond, M. K.; Myrick, M. L. *Acc. Chem. Res.* **1989**, *22*, 364.

(50) DeArmond, M. K. *Acc. Chem. Res.* **1974**, *7*, 309.

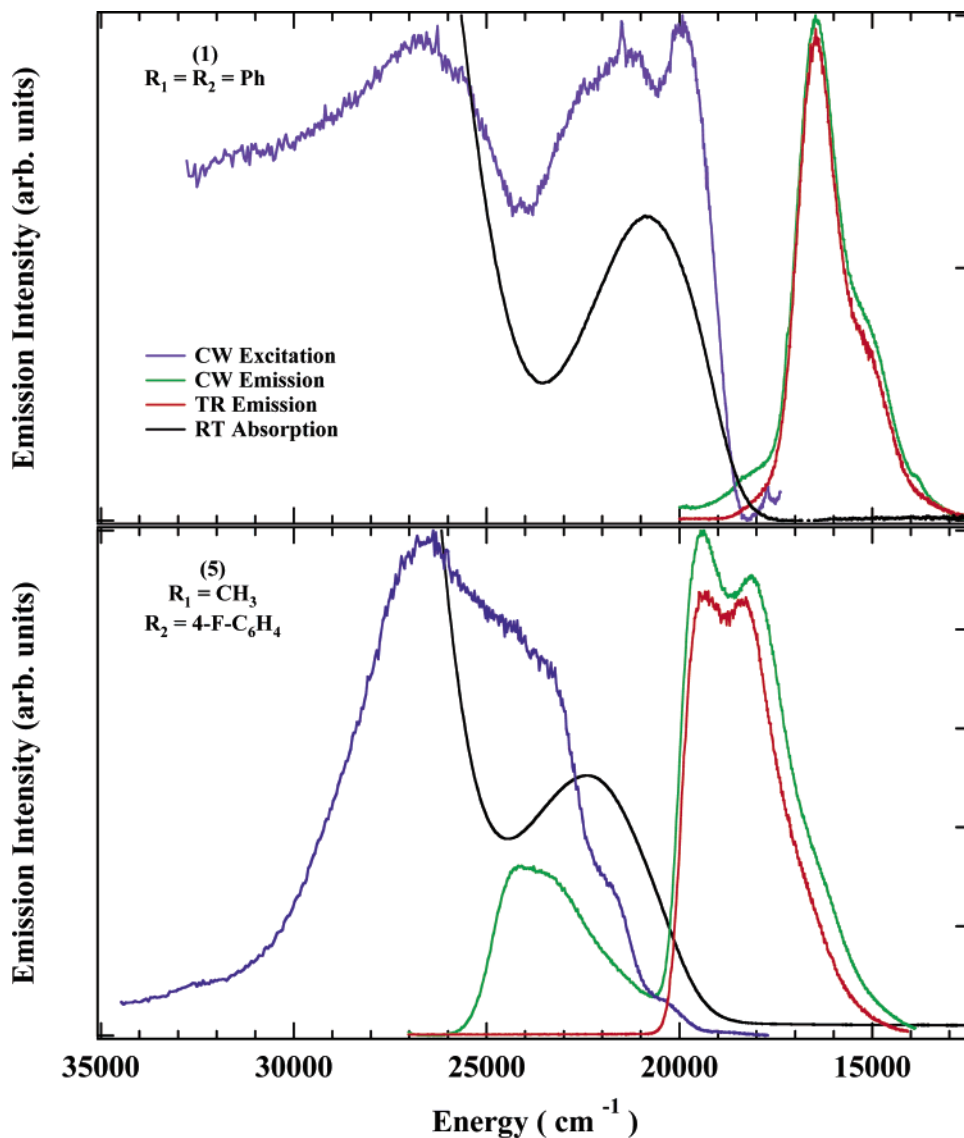


Figure 7. 77 K Emission spectral data obtained for toluene glasses of complexes $(C_5Me_5)_2Th[-N=C(R_1)(R_2)]_2$ **1** (top) and **5** (bottom). Spectral parameters used for **1** were as follows: CW emission: $\lambda_{em} = 450$ nm (22220 cm^{-1}), CW excitation: $\lambda_{em} = 600$ nm (16670 cm^{-1}), TR emission: $\lambda_{ex} = 450$ nm (22220 cm^{-1}), delay time = 20 μs , gate width = 1 ms. Spectral parameters used for **5** were as follows: CW emission: $\lambda_{ex} = 365$ nm (27400 cm^{-1}), CW excitation: $\lambda_{em} = 575$ nm (17400 cm^{-1}), TR emission: $\lambda_{ex} = 360$ nm (27780 cm^{-1}), delay time = 60 μs , gate width = 1 ms.

complexes. Note that the higher-energy, shorter-lived emission band (Figure 7, bottom) corresponds more closely in energy to that of the two states in the singlet manifold from the absorption spectrum. This is *prima facie* evidence that the lowest-energy absorbing and higher-energy emitting states are the same, namely the lowest-lying singlet state(s). It is also possible to observe the identical lower-energy emission band in all these multiple-emitting complexes by pumping directly into the region of the higher-energy emission band (not shown in Figure 7). This demonstrates that these two emissive states are strongly coupled as expected for singlet/triplet pairs of the same orbital parentage. Finally, we note that even the nitrile precursors exhibit multiple-state emission from both singlet and triplet manifolds. This behavior is well documented in the literature for benzonitrile for which the ratio of singlet to triplet emission intensity is strongly medium dependent.^{51,52} This observation has been confirmed for all the nitrile precursors used in this

study (Supporting Information). Note, however, that the excited states in the nitrile precursors are $\pi\pi^*$ in character in contrast to the $n\pi^*$ character in the ketimide complexes. On the whole, the evidence seems to best support the assignment of the two observed emitting states in the thorium bis(ketimide) complexes as being ketimide $n\pi^*$ singlet (S_1) and triplet (T_1) in character.

While emission from the S_1 state is not directly observed in complexes **1** and **11**, it is nonetheless possible to locate this state in the emission excitation spectrum (Figure 7, top) as the lowest-lying state from which the triplet emission is excited. A complete summary of the S_1 and T_1 state energies from the 77 K emission data is provided in Table 6. All emission and emission excitation bands are vibronically resolved. However, the extent of the resolution at this temperature is not high, so precise locations of the S_1 and T_1 electronic origins (E_{00}) are not possible. The data in Table 6 are derived from the apparent

(51) LeBel, G. L.; Laposa, J. D. *J. Mol. Spectrosc.* **1972**, *41*, 249.

(52) Mordzinski, A.; Sobolewski, A. L.; Levy, D. H. *J. Phys. Chem. A* **1997**, *101*, 8221.

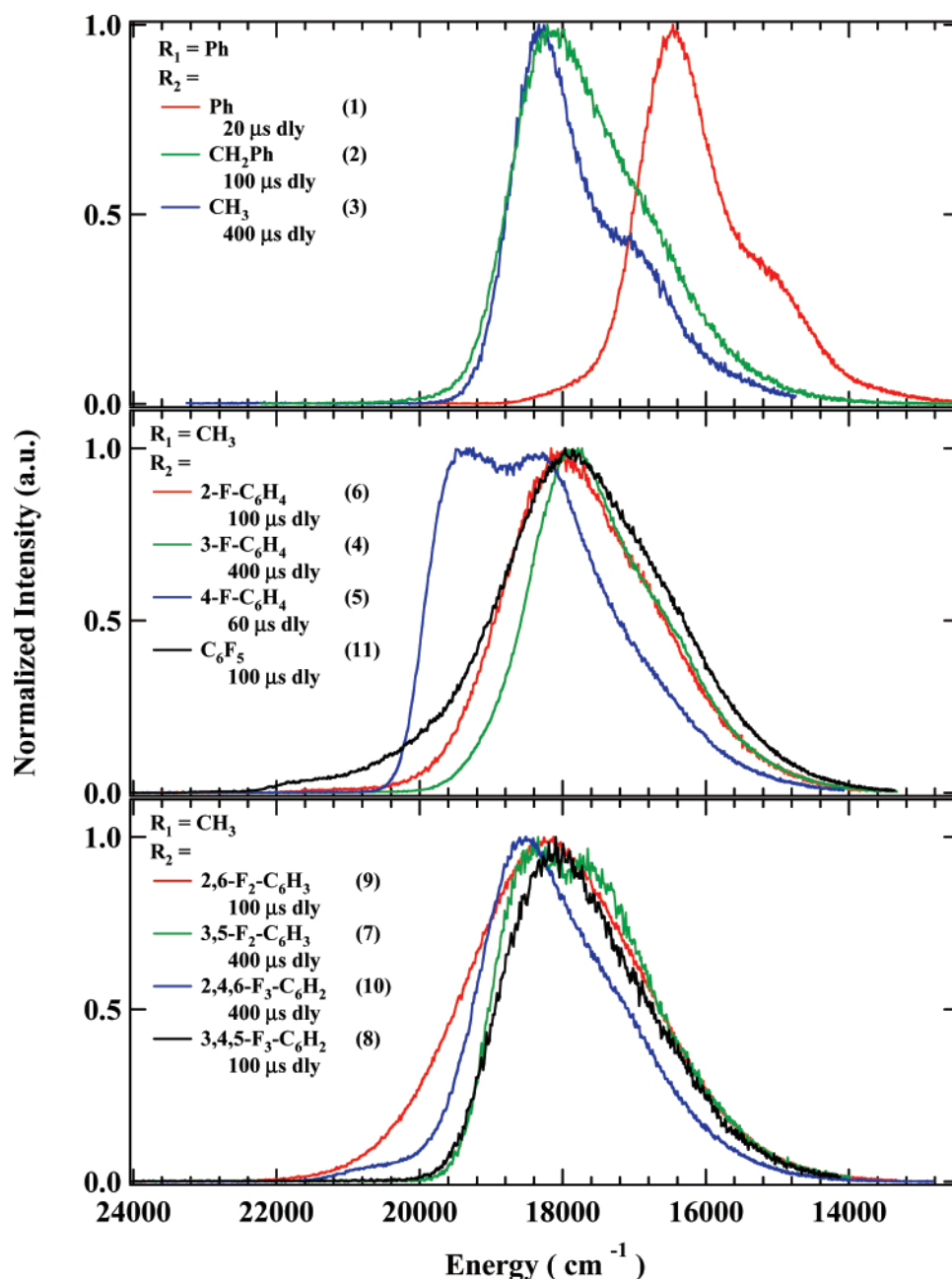


Figure 8. Time-resolved emission spectra from the nominal T_1 excited-state for $(C_5Me_5)_2Th[-N=C(R_1)(R_2)]$ complexes in toluene glass at 77 K. All spectra were collected using a 1-ms gate width and a gate delay as indicated in the legends.

energy of the highest-energy vibronic band in each manifold. In the previous TD-DFT study, the energies of the lowest triplet states were also determined for the model complex **1a**, and the calculated values (nearly degenerate pair at 2.4 eV or 19350 cm^{-1}) are in good agreement with those observed for $(C_5Me_5)_2Th[-N=C(Ph)_2]$ (**1**).

A complete summary and comparison of the triplet emission spectra for complexes **1–11** are provided in Figure 8. The spectra are all derived from time-resolved data collection at 77 K. As with absorption spectra shown in Figure 6, these triplet emission data illustrate the range of electronic energies found in this series of ketimides. Measured emission lifetimes have also been determined for this complete series of complexes by collecting emission decay data on the red edge of these triplet spectral bands while exciting at energies

greater than the S_1 energy for each system.⁵³ In all cases, the measured decay curves were adequately fit using a two-exponent function comprising a very short lifetime (attributed to the instrument response function) and a long lifetime assigned to the measured lifetime of the complex. The lifetime data are summarized in Table 6. Note that there is very little dispersion (~ 150 – $400 \mu s$) in these measured lifetime values except for complex **1**, which has a much shorter ($\sim 50 \mu s$) lifetime. This shorter lifetime may simply be a consequence of the energy-gap law⁵⁴ since the emission energy for **1** is so much lower than that of the other thorium ketimide complexes. Even for a ligand-based emission, these measured lifetimes are

(53) These samples are all rigorously oxygen-free since they were prepared in an inert atmosphere drybox using deoxygenated solvents. Thus, excited-state lifetimes are not impacted by quenching from oxygen.

(54) Forster, L. S. *Coord. Chem. Rev.* **2002**, 227, 59.

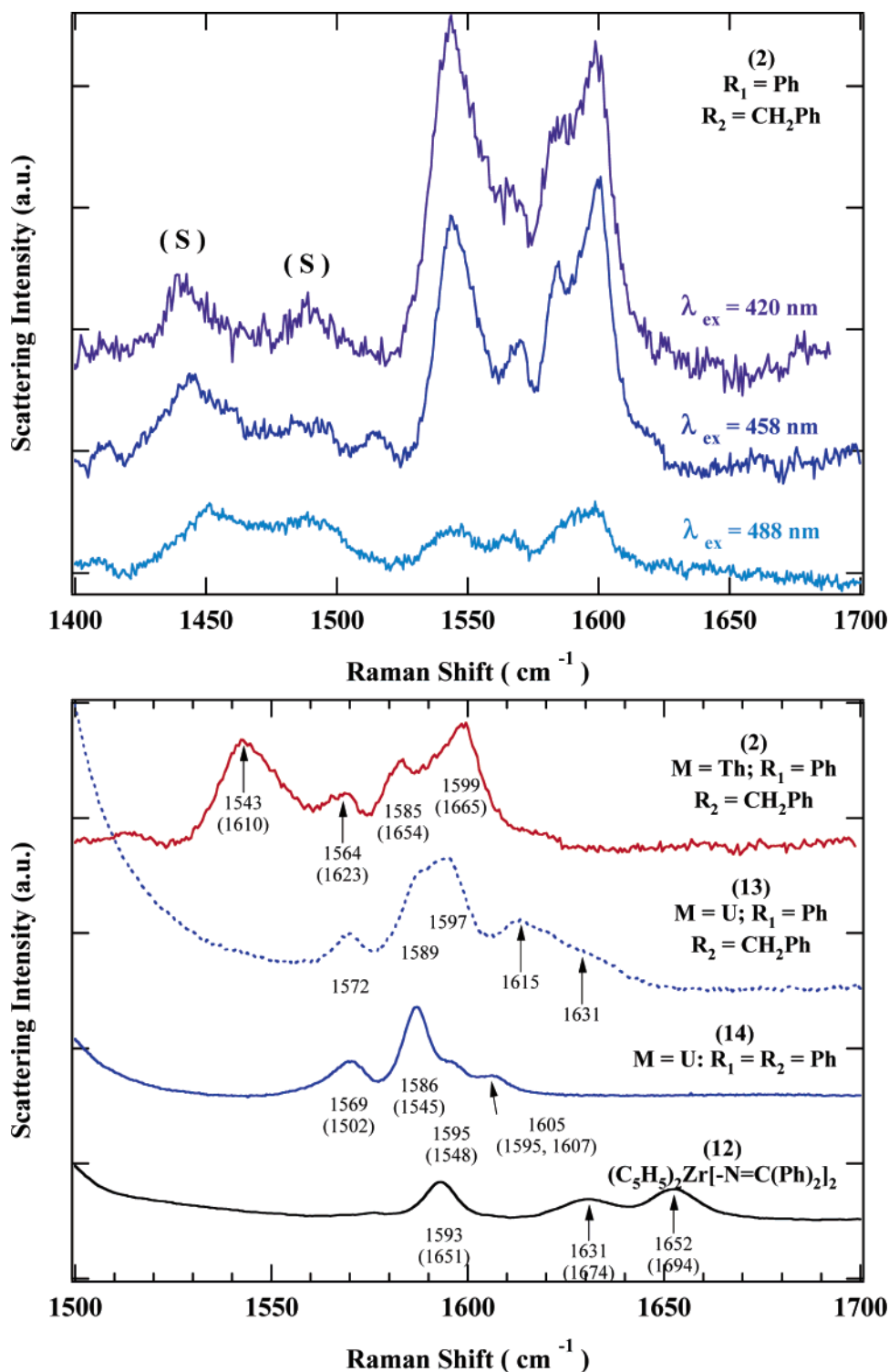


Figure 9. Resonance Raman vibrational spectra for $\sim 10 \text{ mM}$ solutions of $(\text{C}_5\text{H}_5)_2\text{M}[\text{N}=\text{C}(\text{R}_1)(\text{R}_2)]_2$ complexes in THF at room temperature. Top panel: Excitation-wavelength dependence in the resonance-enhanced Raman spectra of **2** in the region of the ketimide C=N and phenyl C=C modes. Solvent bands are labeled "(S)". Bottom panel: Raman spectral comparison among bis(ketimide) complexes. Complex **2** at 458 nm, **13** at 514 nm, **14** at 514 nm, and **12** at 458 nm. Modes dominated by C=N stretching are indicated with arrows. Band positions (in cm^{-1}) are indicated for $\nu_{\text{C}=\text{C}}$ and $\nu_{\text{C}=\text{N}}$ modes. Values in parentheses are from DFT calculations (ref 3). Data for **12–14** are taken from ref 3.

surprisingly long; particularly so since a high Z metal is in intimate contact with the emitting chromophore. Presumably the long lifetimes are at least in part a consequence of both orbital and spin-forbidden nature of the $^3n\pi^*$ state, and as noted above, the Th atom may actually serve to facilitate the excited-state relaxation. We were unable to measure comparable emission lifetimes while monitoring emission within the putative

S_1 band because the temporal resolution of our instrument ($\sim 20 \mu\text{s}$) was insufficient to capture this very short lifetime of this state.

The triplet spectra also exhibit varying degrees of vibronic structure. For those systems for which this structure is most evident, it appears that most of the intensity resides in the first (highest-energy) vibronic band. As noted above, the apparent

vibronic spacings in these triplet emission spectra do not correspond to real vibrational modes of the complexes. Instead, they represent a time-domain weighted average of mode energies and displacements in the excited electronic states.^{35–37} However, the observation that the greatest intensity appears in the first apparent vibronic band is consistent with the conclusion that the distortion between the ground state and T_1 along the normal mode(s) responsible for this vibronic structure is not particularly large, again consistent with nonbonding to antibonding ($n\pi^*$) character of the excited state.

Resonance Raman Spectroscopy. The final noteworthy spectral property observed for the thorium systems is resonance enhanced Raman scattering. This behavior is perhaps anticipated, given the vibronic structure seen in the low-temperature absorption and emission spectral data. Such vibronic structure is a hallmark of Franck–Condon activity in one or more vibrational modes between the ground and excited electronic states, and this is the primary mechanism giving rise to enhancement in the Raman spectrum. This novel resonance Raman behavior has been previously noted for several U(IV) and Zr(IV) bis(ketimide) complexes,⁵ but there is no known precedent for this behavior in the literature of Th(IV) chemistry. The observation of resonance Raman scattering is a much greater experimental challenge in the case of the thorium complexes than in the analogous uranium systems, because all the thorium bis(ketimide) compounds are intensely emissive in the same spectral region that is probed in the resonance Raman experiment.⁵⁵ Thus, our studies to date have been limited to complex **2**, which is a somewhat weaker emitter than the other thorium bis(ketimide) complexes.

Typical resonance Raman spectral data for ~ 10 mM complex **2** in THF solution are illustrated in Figure 9. The top panel shows the intensity profile in the region of the C=N and C=C stretching modes as the excitation wavelength is tuned into resonance with the $n\pi^*$ singlet manifold and the higher-lying $\pi\pi^*$ state(s). These data also confirm the resonance enhanced nature of the scattering since (1) the intensities in the complex modes are equal to or exceed those of the THF modes (indicated by “(S)” in Figure 9, top) for a solution that is ~ 10 mM in **2** but ~ 12 M in solvent (i.e., $\sim 10^3$ difference in concentration of scatterers), and (2) the intensity in the complex modes increases as the excitation is tuned further into the absorption envelope (Figure 6).

A comparison of this same spectral region for **2** and several U(IV) and Zr(IV) bis(ketimide) complexes is provided in the lower panel of Figure 9. Most notable in this comparison is the fact that the energies of the two principally C=N stretching modes for **2** have shifted to significantly lower energy than those observed for the same two modes in $(C_5Me_5)_2U[-N=C(Ph)-(CH_2Ph)]_2$ (**13**), while the energies of the principally C=C (phenyl) stretching modes remain at about the same energy between the two complexes (Figure 9B, complex **2**). This

general trend in the energy of these two sets of modes ($\nu_{C=N}$ and $\nu_{C=C}$) was also obtained in previously reported DFT calculations.¹¹ This observation indicates that the C=N bonds in **2** are weakened relative to the same bond strengths in the uranium analogue, and the implication is that there may be stronger metal–nitrogen bonding in the thorium complex than in the analogous uranium complex that pulls some of the electron density from the C=N bonds, leading to their weakening. Such an effect could easily be envisioned to arise from explicit involvement of the metal 6d orbitals in ligand bonding. This involvement should be greater in thorium than uranium because of the relative lower energy of the 6d orbitals in the thorium system. The proposed strengthening of the Th–N bond should also be manifest in the vibrational data, but the energy of these metal–ligand stretching modes are expected to be quite low, and we are unable to unambiguously identify them in our spectral data.

Conclusions

This systematic investigation of the structural and electronic effects of fluorine substitution on the phenyl ring (Ar_F) in the ketimide ligands of $(C_5Me_5)_2Th[-N=C(CH_3)(Ar_F)]_2$ complexes has revealed a substantial impact on both the structural chemistry and the physical data (spectroscopy and electrochemistry) that report on the electronic structure in this series of complexes. We do not observe a strong correlation among the spectroscopic or electrochemical data for this series that would suggest a dominant influence from the variation in the fluoride substitution pattern. Nonetheless, we do find excellent agreement in both the structural chemistry and the electronic energy levels between experiment and density functional theory calculations. Clearly, there are multiple factors at play in this series of complexes, most notably the structural distortions that accompany the fluoride substitution at both ortho positions on the aryl ring for complexes **9–11**, that likely mask any simple trends resulting from inductive effects.

Acknowledgment. For financial support of this work, we acknowledge the LANL Glenn T. Seaborg Institute for Transactinium Science (Postdoctoral fellowships to E.J.S., P.Y., and R.E.D.; summer research fellowship to K.C.J.), LANL (Director’s Postdoctoral Fellowship to E.J.S.), the LANL Laboratory Directed Research and Development Program, and the Division of Chemical Sciences, Office of Basic Energy Sciences, Heavy Element Chemistry program. This work was carried out under the auspices of the National Nuclear Security Administration of the U.S. Department of Energy at Los Alamos National Laboratory under Contract No. DE-AC52-06NA25396.

Supporting Information Available: Full synthetic details and characterization data for complexes **4–11**, X-ray structural data and tables for complexes **5–11**, details of the DFT calculations and absorption and emission data for complexes **1** and **12**, and emission data for some nitriles. This material is available free of charge via the Internet at <http://pubs.acs.org>.

JA0686458

(55) The analogous uranium complexes do not emit, even at 77 K, presumably because the lower-lying manifold of ligand field states are very efficient at non-radiatively relaxing the otherwise emissive ligand-based excited states.